
LEARNING DYNAMICS AND STRUCTURE OF COMPLEX SYSTEMS USING GRAPH NEURAL NETWORKS

A PREPRINT

Zhe Li ^{*,1,3}

¹ Department of Neuroscience
Baylor College of Medicine
zhe1@bcm.edu

Andreas S. Tolias ^{1,2,3}

² Department of Electrical and Computer Engineering
Rice University

Xaq Pitkow ^{*,1,2,3}

³ Center for Neuroscience and Artificial Intelligence
Baylor College of Medicine
xaq@rice.edu

February 23, 2022

ABSTRACT

Many complex systems are composed of interacting parts, and the underlying laws are usually simple and universal. While graph neural networks provide a useful relational inductive bias for modeling such systems, generalization to new system instances of the same type is less studied. In this work we trained graph neural networks to fit time series from an example nonlinear dynamical system, the belief propagation algorithm. We found simple interpretations of the learned representation and model components, and they are consistent with core properties of the probabilistic inference algorithm. We successfully identified a ‘graph translator’ between the statistical interactions in belief propagation and parameters of the corresponding trained network, and showed that it enables two types of novel generalization: to recover the underlying structure of a new system instance based solely on time series observations, or to construct a new network from this structure directly. Our results demonstrated a path towards understanding both dynamics and structure of a complex system and how such understanding can be used for generalization.

Keywords Graph neural network · Belief propagation

1 Introduction

Many real world problems involve dynamical systems composed of interacting parts, such as planet movement, social networks, protein folding, neural circuits, electrical grids, etc. While a system can show complex and rich behavior, the elementary rules about the interaction are usually much simpler. The ability to abstract these simple rules from complex dynamics is one hallmark of intelligence, as it is a key feature of understanding.

When modeling such a dynamical system, we can usually exploit the underlying symmetry and impose certain canonical assumptions on the model. Graph neural networks (GNN) explicitly model each part of the system, and use local messages to model the interaction among them [1, 2, 3, 4]. While GNN framework has been used to study a variety of dynamical systems [5, 6, 7], commonly it is used for modeling one specific instance of the system [8, 9]. As a result it is not trivial to disentangle the different aspects of the learned system, and interpret components of the trained model [10]. In this study, we propose to model multiple instances of the same type of system, and explicitly learn the universal dynamics which are shared across all instances, as well as the specific structure of each individual one. We analyze to disentangle these two aspects of the learned GNN models and show how this understanding enables generalization to new problem instances.

We choose the belief propagation (BP) algorithm on probabilistic graphical model (PGM) as the dynamical system of interest. BP performs probabilistic inference on a set of random variables and their statistical interactions via iterative computations. The algorithm itself is an important operation as it marginalizes out nuisance variables efficiently (approximately for loopy graphs), which is useful in many situations. Given the time series of BP outputs, we aim to understand how they change over time (dynamics) and to recover the underlying PGM (structure).

In this report, we begin by introducing the mathematical definition of GNNs used in our work. We next show the results of fitting GNN models to the BP outputs on multivariate Gaussian distributions, and analyze the representation and components of trained models. We then develop ‘graph translator’ that links between the structural parameters of GNN models and static properties of Gaussian distributions, and show how it enables two types of generalization to new PGM instances. Lastly, we discuss the limitations and future directions of our approach.

2 Background

2.1 Graph neural network

A graph neural network [2, 1, 3] is a message-passing algorithm defined over a graph $\mathcal{G} = (\mathcal{V}, \mathcal{E})$ with vertices \mathcal{V} and edges \mathcal{E} . For a graph of size N , $\mathcal{V} = \{1, \dots, N\}$ and $\mathcal{E} \subseteq \{(i, j) \mid (i, j) \in \mathcal{V}^2 \wedge i \neq j\}$ where (i, j) represents a directed edge from vertex j to i . Each vertex i is associated with a vertex parameter \mathbf{v}_i , and each edge (i, j) is associated with an edge parameter \mathbf{e}_{ij} . We assume that all vertex parameters \mathbf{v}_i are of the same dimension D_v , and all edge parameters \mathbf{e}_{ij} are of dimension D_e .

We use GNNs to model observations of a dynamical system at discrete time points. At each time point t , vertex i receives a D_x -dimensional input \mathbf{x}_i^t . We take D_x to be the same for all vertices, and can be 0 to represent purely autonomous dynamics of a system. The state of vertex i at time t is denoted as \mathbf{s}_i^t , which is a vector of dimension D_s . Vertex states get updated by both time-varying inputs (when $D_x > 0$) and the lateral interaction from neighboring vertices in the form of messages.

Along the edge (i, j) , a pairwise message \mathbf{m}_{ij}^t of dimension D_m is generated by a message function $\mathcal{M}(\cdot)$,

$$\mathbf{m}_{ij}^t = \mathcal{M}(\mathbf{s}_i^t, \mathbf{s}_j^t; \mathbf{e}_{ij}, \Theta_{\mathcal{M}}), \quad (1)$$

in which $\Theta_{\mathcal{M}}$ is a global parameter vector of $\mathcal{M}(\cdot)$. All incoming messages on vertex i are then aggregated via an aggregation function $\mathcal{A}(\cdot)$,

$$\mathbf{m}_i^t = \mathcal{A}(\{\mathbf{m}_{ij}^t \mid (i, j) \in \mathcal{E}\}). \quad (2)$$

$\mathcal{A}(\cdot)$ takes the set of pairwise messages as input, ignoring their order, hence it is permutation invariant. Simple choices of $\mathcal{A}(\cdot)$ include element-wise summation and max pooling, while more complicated mechanisms such as attention-based aggregation can also be used [11, 12]. We choose summation in this study. Finally, the vertex state is updated by an update function $\mathcal{U}(\cdot)$,

$$\mathbf{s}_i^{t+1} = \mathcal{U}(\mathbf{s}_i^t, \mathbf{x}_i^t, \mathbf{m}_i^t; \mathbf{v}_i, \Theta_{\mathcal{U}}), \quad (3)$$

where $\Theta_{\mathcal{U}}$ is a global parameter vector of $\mathcal{U}(\cdot)$. The GNN output is the projection of states via a readout function. Two types of readout function are often applied to the model: a shared readout $\mathcal{R}(\cdot)$ that applies to every vertex separately,

$$\mathbf{o}_i^t = \mathcal{R}(\mathbf{s}_i^t; \Theta_{\mathcal{R}}), \quad (4)$$

or a mixed readout of all vertices,

$$\mathbf{o}^t = \mathcal{R}(\mathbf{s}_1^t, \dots, \mathbf{s}_N^t; \Theta_{\mathcal{R}}), \quad (5)$$

where $\Theta_{\mathcal{R}}$ is a parameter vector of $\mathcal{R}(\cdot)$. The mixed readout is more general in the sense that it does not require knowledge on the number of objects in the system, however it is much more difficult to handle. We will focus on the shared readout in this study, which is useful for computing the marginals for each variable in a PGM.

There is an intrinsic degeneracy among $\mathcal{M}(\cdot)$, $\mathcal{U}(\cdot)$ and $\mathcal{R}(\cdot)$: the complexity of one function may be compensated by the other two. In this study, we use simple linear readouts, so all nonlinearities must be captured by message and update functions. We also assume the readout function $\mathcal{R}(\cdot)$ does not depend on vertex parameters \mathbf{v}_i .

2.2 Belief propagation on probabilistic graph models

A probabilistic graph model (PGM) describes a joint distribution of N random variables $\theta_1, \dots, \theta_N$. Here we focus on PGMs with pairwise interactions. In a graph of size N , each vertex i is associated with a singleton potential $\phi_i(\theta_i)$, and

each undirected edge (i, j) is associated with a pairwise potential $\psi_{ij}(\theta_i, \theta_j)$. The joint distribution of $\theta_1, \dots, \theta_N$ is proportional to the product of all potentials,

$$p(\theta_1, \dots, \theta_N) \propto \prod_{i \in \mathcal{V}} \phi_i(\theta_i) \cdot \prod_{(i,j) \in \mathcal{E}} \psi_{ij}(\theta_i, \theta_j). \quad (6)$$

Marginalization of the joint distribution is one of the most used computation in statistical analysis, and many different methods have been developed for it, including belief propagation (BP), which is an iterative algorithm that operates on a PGM. At each time point t , BP estimates the marginal distribution $p_i(\theta_i)$ as $\hat{p}_i^t(\theta_i)$. BP is not guaranteed to converge, and even when it converges it is not guaranteed to converge to the true marginal distribution, however it provides a decent estimation in many cases [13, 14].

To make the BP dynamics more interesting, we use time-varying singleton potentials $\phi_i^t(\theta_i)$ while keeping the pairwise potential $\psi_{ij}(\theta_i, \theta_j)$ constant. This simulates a system with time-varying local evidence while the coupling among different parts is fixed. BP output $\hat{p}_i^t(x_i)$ therefore is the continuous estimate of $p_i^t(\theta_i)$ determined by $\phi_i^t(\theta_i)$ and $\psi_{ij}(\theta_i, \theta_j)$.

3 Related work

GNNs have been widely used to model time series of physical systems, often about predicting trajectories of interacting objects. In [15, 9, 16], the adjacency matrix of the interaction graph is determined by spatial proximity instead of being learned from data, therefore are not applicable for systems in which ‘neighborhood’ is not clearly defined for instance probabilistic inference. [15] demonstrates GNN can extrapolate to new environments containing more objects, but the structural properties of the system, namely the mass, is the same for all objects and environments.

[15] uses GNNs to infer latent properties such as object mass. Similarly, [7] uses GNN to infer interaction type in a multi-object system. However, the vertex and edge properties in these studies are designed as discrete values. Our work instead investigates a spectrum of continuous graph properties and reveals the intrinsic low-dimensional structure of them.

[10] encourages a GNN model to learn compact internal representation, and performs symbolic regression based on it. Our work reveals low-dimensional structure of GNNs also through regularization. One difference is we view states and messages as a vector instead of individual components, hence avoid the loss of information when representation is not perfectly factorized. Also, we manage to disentangle the structural properties of the system (e.g. mass, charge) instead of assuming they are known. The graph translator proposed in our work can be seen as a more general form of symbolic regression which enables generalization to new instances of complex system.

Besides modeling physical systems, past work has used GNNs for probabilistic inference [17, 18]. GNN is often proposed as a better alternative to traditional BP algorithm, especially on loopy graphs [19] or when higher-order statistics is critical [20, 21]. Our work instead focuses on using GNN to model BP algorithm as a dynamical system, whether it produces accurate probabilistic inference is outside our scope.

4 Methods

4.1 Canonical functions with graph parameters

We say that the message function $\mathcal{M}(\cdot)$, the update function $\mathcal{U}(\cdot)$ and the readout function $\mathcal{R}(\cdot)$ are canonical functions because they are shared across all parts of the graph, or even across multiple graphs of the same general type. $\mathcal{M}(\cdot)$ can be considered to be a family of functions parameterized by the static edge properties e_{ij} , and $\mathcal{U}(\cdot)$ form a family of functions parameterized by vertex properties v_i . To give the graph parameters greater power to modulate the functions, we formulate $\mathcal{M}(\cdot)$ and $\mathcal{U}(\cdot)$ using a variant of multi-layer perceptron (MLP), called meta-MLP. A meta-MLP, or mMLP for short, is simply a standard MLP with the meta-parameter concatenated to each layer’s input. Specifically, the transformation at the l -th layer is

$$\mathbf{x}^{l+1} = f^l \left(\mathbf{W}^l \begin{bmatrix} \mathbf{x}^l \\ \zeta \end{bmatrix} + \mathbf{b}^l \right), \quad (7)$$

where \mathbf{x}^l is the activation of l -th layer and ζ is the meta-parameter shared by all layers. mMLP is a universal function approximator given enough hidden layers and units. More details about the mMLP are in Appendix A.

The message function $\mathcal{M}(\cdot)$ is an mMLP modulated by e_{ij} , and the update function $\mathcal{U}(\cdot)$ is a modified GRU function [22] whose original gate functions are replaced with mMLPs modulated by v_i . More details are in Appendix B.

4.2 Multi-graph training

An important merit of GNN is that the dynamical and structural aspects of a system are represented separately. The canonical functions characterize the dynamics “law” of a certain type of system, such as the BP algorithm, while the graph parameters describe the structure of a particular system instance, *e.g.* the pairwise coupling in a PGM.

Because both aspects affect the system behavior, it is not trivial to disentangle them based on the observations of the system. In order to inspect the effect of different structures while keeping the dynamics fixed, we need a large number of vertices and edges that cover a wide range of parameters, which suggests using a huge graph. However, training GNN on a huge fully connected graph is computationally expensive. Instead, a more feasible approach is to train multiple medium graphs simultaneously. It is equivalent to training on a huge graph with the knowledge that it is a union of several disconnected components.

In this study, we prepare BP traces on multiple PGMs and simultaneously train multiple GNNs corresponding to each. The GNNs share the same canonical functions but different graph parameters for each individual PGM. The training objective function is simply the summation of loss function over all PGMs (Fig. 1). Each individual loss is designed to be proportional to the amount of data, therefore the trained canonical functions are naturally biased towards the PGMs with more training data.

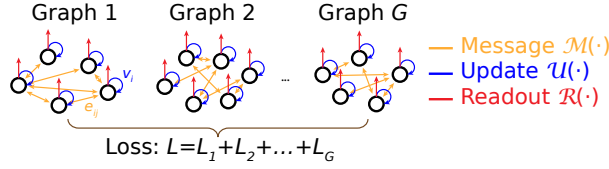


Figure 1: Schematic of multi-graph training. While each GNN has its own graph parameters, the canonical functions are shared by all. Canonical functions and graph parameters represent the dynamical and structural aspects of the system, respectively.

We categorize the GNN parameters as dynamical parameters $\Theta^D = \Theta_M \cup \Theta_U \cup \Theta_R$ and structural parameters $\Theta^S = \{e_{ij}\} \cup \{v_i\}$. Denoting the number of GNN models as G , we need to learn one set of shared dynamical parameters Θ^D , and G sets of structure parameters $\Theta_1^S, \dots, \Theta_G^S$ for each PGM respectively.

4.3 Problem formulation

In this work, we study the BP algorithm on a time-varying multivariate Gaussian distribution defined by

$$\phi_i^t(\theta_i) = \exp\left(-\frac{a_i}{2}\theta_i^2 + b_i^t\theta_i\right), \quad (8)$$

$$\psi_{ij}(\theta_i, \theta_j) = \exp(-J_{ij}\theta_i\theta_j). \quad (9)$$

The joint distribution $p(\theta)$ can be rewritten as

$$p(\theta) \propto \exp\left(-\frac{1}{2}\theta^\top A\theta + b^t\theta\right), \quad (10)$$

with $A_{ii} = a_i$, $A_{ij} = A_{ji} = J_{ij}$ as the precision matrix. The bias time series b^t is a sequence of constant values with random duration following a Poisson process, while switching between periods are smoothed by a Hamming window.

Since the marginal distributions $p_i(\theta_i)$ are also Gaussian distributions, BP on Gaussian distribution [23] returns its single-variable means μ_i^t and standard deviations σ_i^t , *i.e.*,

$$\hat{p}_i^t(\theta_i) \propto \exp\left(-\frac{1}{2\sigma_i^{t2}}(\theta_i - \mu_i^t)^2\right). \quad (11)$$

When converged, these means are exact but the standard deviations are approximate for loopy graphs [24]. We use a damped version of the BP algorithm and add processing noise at each time step. The damping parameter is adjusted so that transient dynamics makes up a significant portion of the full trial. When the precision matrix A is constant, the estimated standard deviation σ_i^t quickly converges to the true value $\frac{1}{\sqrt{a_i}}$ independent of any time-dependent bias terms, so we focus on μ_i^t only. An example trial of BP trace is shown in Fig. 2.

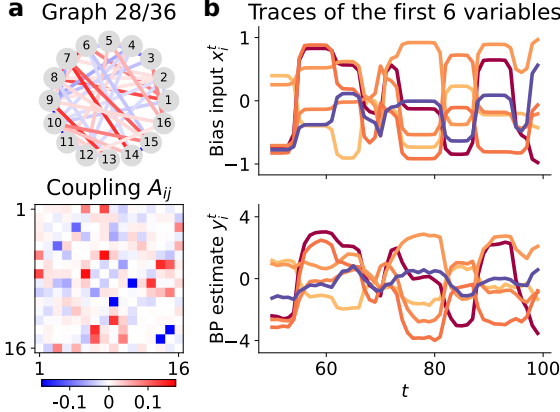


Figure 2: Traces by BP algorithm on a multivariate Gaussian distribution. (a) One example of the 36 PGMs, containing 16 random variables. Only the off-diagonal part of precision matrix \mathbf{A} is shown, characterizing the coupling among variables. (b) Bias sequence b_i^t (Eq. 8) serves as the input to GNN models, and the noisy BP estimation of marginal mean μ_i^t (Eq. 11) is the target for GNN output to fit. Each variable is plotted with a different color.

The inputs to GNN are $\mathbf{x}_i^t = [b_i^t]$, and the targets for the GNN to match are defined as $\mathbf{y}_i^t = [\mu_i^t]$. The GNN output \mathbf{o}_i^t (Eq. 4) is constructed to have the same dimension as \mathbf{y}_i^t , in this case of dimension 1. We use the squared error $L = \sum_{i,t} \|\mathbf{o}_i^t - \mathbf{y}_i^t\|^2$ as the loss function. As introduced in Sec. 4.2, the losses on all PGMs are summed up as the overall objective function. In practice, each training batch is fetched from a randomly selected PGM.

Our loss includes L_2 regularization on the structural parameters $\Theta^S = \{e_{ij}\} \cup \{v_i\}$, which turn out to be critical in disentangling Θ^S from Θ^D (see Section 5.5).

BP traces for 36 random PGMs are generated, using different number of variables, number of trials and time duration for each. The graph density and coupling strengths are approximately the same for all PGMs. More details can be found in Appendix D.

5 Results

5.1 Architecture comparison

The GNN architecture is determined by various hyper-parameters, including the underlying graph connectivity \mathcal{E} , the dimensions D_v , D_e , D_s , D_m , and hidden layer sizes of canonical functions $\mathcal{M}(\cdot)$ and $\mathcal{U}(\cdot)$. We study the effect of hyper-parameters by performing an extensive search of model configurations and comparing the fitting quality of the trained GNNs. We first define a set of possible values for each hyper-parameter, randomly choose combinations for a GNN architecture, and find the best architecture conditioned on each value to examine the effect of this hyper-parameter. For example, if the candidate values for edge dimension D_e are $\{0, 2, 4, 8\}$, the best architectures found by hyper-parameter search conditioned on each D_e value are compared.

The graph connectivity \mathcal{E} is treated as a hyper-parameter because it is difficult to learn it in an end-to-end manner. Without any prior knowledge of the structure of a system, the only fair choices are a null graph ($\mathcal{E} = \emptyset$) or a complete graph ($\mathcal{E} = \{(i, j) \mid (i, j) \in \mathcal{V}^2 \wedge i \neq j\}$). The former ('null') assumes no coupling among variables, while the latter ('full') assumes all pairs of coupling are possible. Not surprisingly, 'full' GNNs fit data better than 'null' GNNs (Fig. 3a), demonstrating the necessity of pairwise messages for explaining the traces in our BP example. It is worth mentioning that even the 'null' GNNs produce good fit ($R^2 = 0.923$), because BP estimates μ_i^t in this example are largely determined by the singleton potentials $\phi_i(x_i)$ and only slightly 'pulled' by other variables. The reason for using the moderately coupled system is to avoid numerical instability of BP.

We next examine the effects of model component dimensions, including D_v , D_e , D_s and D_m . The results (Fig. 3a) show that a non-zero edge dimension is critical in fitting the BP traces on Gaussian distribution; the real coupling is a scalar and thus of dimension 1. Surprisingly, the vertex dimension does not have to be greater than zero, even though the precision parameter A_{ii} is a vertex attribute of dimension 1. We will discuss how to identify ground truth dimension through graph translators in Section 6. There is a small benefit of increasing state dimension D_s , but no significant

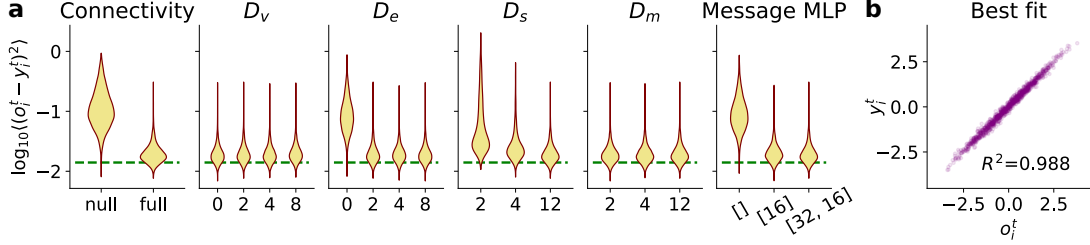


Figure 3: GNN architecture comparison and the best trained model. (a) The distribution of log mean squared errors (MSE) in the held-out testing set for the best GNN conditioned on each hyper-parameter value. Graph connectivity \mathcal{E} , vertex dimension D_v , edge dimension D_e , state dimension D_s , message dimension D_m and the hidden layer size of message function $\mathcal{M}(\cdot)$ are examined. Dashed line is the baseline performance, which is the median of MSE if noiseless BP traces is treated as prediction. (b) BP target y_i^t against GNN output o_i^t of the best trained model.

effect of message dimension D_m . It should be noticed that the best architecture for each conditioned value is usually different. For example, the best configuration is $(D_v = 0, D_e = 8)$ for $D_m = 2$ and $(D_v = 4, D_e = 1)$ for $D_m = 12$.

Lastly we examine the effect of message function complexity characterized by the hidden layer sizes in $\mathcal{M}(\cdot)$, and find that nonlinearity in the message is crucial for GNNs to fit well (Fig. 3a).

Due to the high cost of hyper-parameter search, we do not compare different update functions, but fix it to a GRU function modulated by the vertex parameter v_i . A more thorough search is left for future work.

To summarize, the results show strong dependency of fitting quality on graph connectivity, edge dimension and the message function nonlinearity, which indicates that in order to fit this dataset well, nonlinear messages between vertices are essential, and the GNN edges need to be parameterized.

5.2 GNN training result

One of the best architecture we find uses ‘full’ connectivity, $D_e = 2, D_v = 2, D_h = 12, D_m = 12$ and a message function with one hidden layer of size 16. After a short initial burn-in period, the outputs of the trained GNNs faithfully reproduce the BP traces on the held-out testing set ($R^2 = 0.988$, Fig. 3b). Not only do the GNN outputs reach the same equilibrium as BP targets within each input period, but the temporal profile at each input switch is also accurate. An example trial is shown in Appendix (Fig. 10).

5.3 State and message manifold

We next analyze the states and messages of this well-trained GNN. We gathered these time series from all graphs and performed principal component analysis (PCA) on them. As expected, GNN states and messages only occupy a small portion of the high-dimensional space. The effective dimension of the manifold is defined as

$$\tilde{D} = \frac{(\sum_i \lambda_i)^2}{\sum_i \lambda_i^2}. \quad (12)$$

where λ_i denotes the variance of the i -th PC. When the state dimension is set to $D_s = 12$, the effective dimension of state manifold is only $\tilde{D}_s \approx 1.74$ (Fig. 4a). We visualize GNN states in 2D and find they are organized by vertices. States at each vertex form its own curved 1D manifold, slightly separated for different vertices (Fig. 4b).

We perform the same analysis on pairwise messages as well. The effective dimension of messages is $\tilde{D}_m \approx 3.37$ for message dimension $D_m = 12$ (Fig. 5a). Different manifolds occupy the message space with different orientations and offsets. Though messages gathered from all edges are not as structured as states, those on individual edges also trace out its own 1D manifold (Fig. 5b). We analyze the dimensionality of aggregated messages \mathbf{m}_i^t (Eq. 2) and find they also lie approximately on a 1D manifold specific to each vertex (Appendix F).

5.4 Interpretable canonical functions

With a clearer picture of the GNN states and messages, we next analyze the learned canonical functions $\mathcal{U}(\cdot)$ and $\mathcal{M}(\cdot)$. We take advantage of the fact that the states and messages conditioned on a vertex or an edge approximately lie on a curved 1-D manifold (Section 5.3). Therefore we can project the states or messages on the leading PC for that vertex or

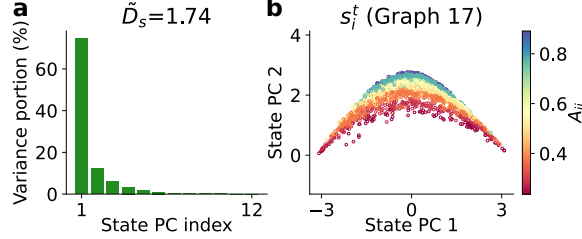


Figure 4: Manifold analysis of GNN states. (a) PCA spectrum of states on all vertices in all GNNs. The effective dimension is $\tilde{D}_s \approx 1.74$ (for $D_s = 12$). (b) Projection of states s_i^t of one GNN onto the space spanned by first two state PCs. Each point is colored by the parameter of vertex it belongs to, *i.e.* the diagonal element of precision matrix A .

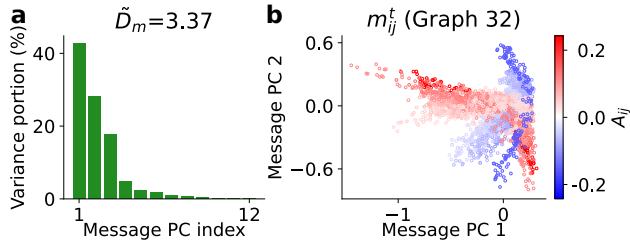


Figure 5: Manifold analysis of GNN messages. (a) PCA spectrum of messages on all edges in all GNNs. The effective dimension is $\tilde{D}_m \approx 3.37$ (for $D_m = 12$). (b) Projection of messages m_{ij}^t of one GNN onto the space spanned by first two message PCs. Each point is colored by the parameter of the edge it travels on, *i.e.* the coupling strength A_{ij} .

edge, and use this projection as a proxy to visualize how these functions depend on their inputs. Although inputs and outputs of $\mathcal{U}(\cdot)$ and $\mathcal{M}(\cdot)$ are vectors, we use scalar proxies as coordinates to plot heat maps of canonical functions (Fig. 6).

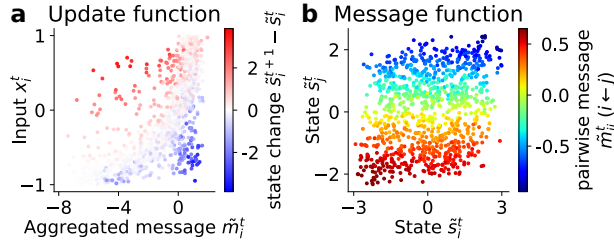


Figure 6: Visualizations of example update and message functions for a randomly selected vertex and edge. Since the high-dimensional states and messages lie on approximately 1-D manifolds, we plot these quantities according to their projection onto their first PCs. (a) State change as a function of aggregated message and the external input. (b) Pairwise message as a function of state at source vertex i and target vertex j .

For a GNN vertex with parameter v_i , the update function $\mathcal{U}(\cdot)$ (Eq. 3) is a function of s_i^t , x_i^t and \mathbf{m}_i^t , in which the \mathbf{m}_i^t is the aggregated message for vertex i at time t . The input x_i^t is the external input, which is simply the local bias b_i^t in this case. We denote the scalar proxies as \tilde{s}_i^t , \tilde{s}_i^{t+1} and \tilde{m}_i^t respectively. We then focus on the state change $\Delta\tilde{s}_i^t = \tilde{s}_i^{t+1} - \tilde{s}_i^t$ as a function of x_i^t and \tilde{m}_i^t . Fig. 6a shows one example, in which the state change $\Delta\tilde{s}_i^t$ is positive when \tilde{m}_i^t is small and x_i^t is large, and is negative otherwise. Hence $\Delta\tilde{s}_i^t$ encodes the discrepancy between aggregated message \tilde{m}_i^t and the external input x_i^t .

For a GNN edge with parameter e_{ij} , the message function $\mathcal{M}(\cdot)$ (Eq. 1) is a function of s_i^t and s_j^t that returns \mathbf{m}_{ij}^t . Again we denote corresponding scalar proxies as \tilde{s}_i^t , \tilde{s}_j^t and \tilde{m}_{ij}^t . It appears that \tilde{m}_{ij}^t changes monotonically with either s_i^t or s_j^t , while depending mostly on the source vertex state \tilde{s}_i^t (Fig. 6b).

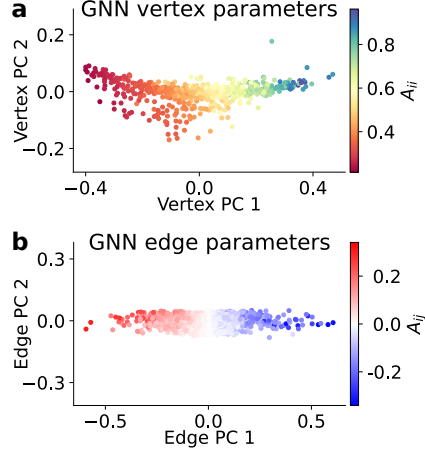


Figure 7: Low-dimensional structure of learned graph parameters. (a) Vertex parameters of dimension $D_v = 2$ from all trained GNNs, colored according to the local precision parameter A_{ii} . (b) Edge parameters of dimension $D_e = 2$ from all trained GNNs, colored according to the coupling strength parameter A_{ij} .

5.5 Graph translator

The structural parameters $\Theta^S = \{e_{ij}\} \cup \{v_i\}$ of each individual GNN are learned independently, and they should relate to the true parameters of the corresponding PGMs. In a multivariate Gaussian distribution, a local precision parameter A_{ii} is associated with each variable, and a coupling strength parameter A_{ij} (Eq. 8–10) is associated with each pair of variables. The hypothesis is that there exists a mapping between GNN vertex parameters v_i and A_{ii} , as well as between GNN edge parameters e_{ij} and A_{ij} . We will learn this mapping between GNN structural parameters and the static attributes of the target nonlinear dynamical system, and term it a ‘graph translator’ because the conversion goes both ways.

Before learning the translators, we first look at the distribution of v_i and e_{ij} . Though $D_v = D_e = 2$ in the trained GNN, both vertex parameters and edge parameters approximately form a 1-D manifold. Moreover, locations on the two manifolds are continuously mapped to the corresponding attributes of PGM (Fig. 7).

The explicit structure that emerges in parameter space depends critically on the regularization of structural parameters during training. Such low-dimensional structure does not show up without the L_2 norm regularization on v_i and e_{ij} . Well-trained but unregularized GNNs still give approximately the same good predictions of BP traces, but the effective dimensionality for vertex and edge parameters are very close to their embedding dimensions of D_v and D_e (Appendix G).

The graph translator we train is simply an MLP with two hidden layers, though it can be any regression model that predicts A_{ii} from v_i (vertex translator) or A_{ij} from e_{ij} (edge translator), or the opposite direction. To quantitatively evaluate graph translators, we divide all G graphs into training, validation and testing sets. Only the original PGM attributes (e.g. A_{ii} and A_{ij}) of training and validation graphs will be used to learn the graph translator, and the testing graphs will be used to evaluate how well the translator behaves. The training graphs are used to train the translator directly, and the validation graphs are only used for early stopping. We also assume it is expensive to obtain the original graph attributes (e.g. in neuroscience applications it is laborious to measure synapse strength by patch-clamping experiments), so we use only a subset of the data in training and validation graphs. Specifically, only 80% of the vertices or edges are randomly selected for training the corresponding graph translator. All vertices and edges in the testing graphs are used for evaluation. In the results below, the training/validation/testing split is 32/2/2 graphs each.

The translated local precision A_{ii} and coupling strength A_{ij} both match the ground truth well, with $R^2 = 0.946$ and $R^2 = 0.867$ respectively (Fig. 8a). Recovered coupling matrix A_{ij} ($i \neq j$) looks similar to the ground truth (Fig. 8b), revealing the correct interactions among different random variables. Since we do not enforce any symmetry about GNN edges e_{ij} , the recovered coupling matrix is not perfectly symmetric. It is straightforward to reveal the underlying structural connectivity between variables by thresholding the coupling strength.

Graph translators can also be used in the reverse direction to directly construct GNN models for a given PGM. The new GNN uses old dynamical parameter Θ^D with the new structural parameter Θ^S translated from precision matrix A . We compare the constructed GNNs with two control models. The first is the best trained colorless GNN with $D_v = D_e = 0$.

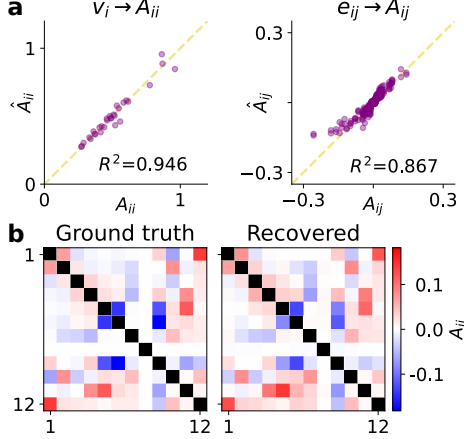


Figure 8: Translating from GNN graph parameters to precision matrix. (a) Both the vertex translator and edge translator predict attributes of PGM on the testing graphs. (b) The coupling matrix A_{ij} recovered by the edge translator closely resembles the ground truth. Diagonal part of A is not shown for better visualization.

Colorless GNNs can be constructed for new PGM directly, without using a graph translator. The second control is the best-trained GNNs with the same parameter dimension as the constructed one, namely the GNNs we obtained earlier for the testing graphs.

The graph parameters of constructed and trained GNNs are close to each other (Fig. 9a). The constructed \hat{v}_i and \hat{e}_{ij} for the testing PGMs are close to the optimal values v_i^* and e_{ij}^* from the corresponding trained GNNs. Although the strong bias terms ensured that even disconnected GNNs would capture some amount of the correct marginals, the colorless GNNs match true traces worst, indicating the benefits of parameterized edges. The trained GNNs match true traces best, since they have access to trace data of the new PGM. The translated GNNs, though never trained on these BP traces, can generate credible traces (Fig. 9b). An example trial from colorless, trained and constructed GNNs are compared against the true BP traces in Fig. 9c.

6 Conclusion and discussions

Using the belief propagation (BP) algorithm on Gaussian probabilistic graph models (PGM) as an example nonlinear dynamical system, we show that graph neural network (GNN) models can be trained on multiple instances of the same type of complex system. Via architecture search, we identify that messages generated by a nonlinear function of states and heterogeneous GNN edges are needed for fitting the BP traces well. We also show that the representation and canonical functions of GNN models have interpretations that are consistent with the principle of probabilistic inference. We further propose the novel concept of a graph translator that links graph parameters in GNN models to graph attributes of the original system. We show that the learned graph translator for Gaussian BP enables two types of generalization: recovering the precision matrix of a new Gaussian PGM from the traces of BP performing inference, and to construct GNN model for a new Gaussian PGM in order to reproduce BP algorithm without knowing its implementation. Unlike generalization to new inputs, such generalization to new instances of the same system builds on the successful disentanglement between dynamics and structure.

We find regularization is crucial to disentangle dynamical parameters $\Theta^D = \Theta_M \cup \Theta_U \cup \Theta_R$ and structural parameters $\Theta^S = \{e_{ij}\} \cup \{v_i\}$. When no regularization is used during GNN training, the learned Θ^S does not show clear structure despite the fact that multiple PGMs are trained together. L_2 norm regularization on vertex and edge parameters v_i and e_{ij} is used in our study, but other options might also work, *e.g.* regularization on states s_i or messages m_{ij} . To our surprise, low-dimensional structure of GNN states s_i and messages m_{ij} is still present when no regularization is used (Appendix G).

Though BP on Gaussian PGM is an important probabilistic inference algorithm, its dynamics are undoubtedly still simple. In future work we would like to test our framework in other complex systems such as celestial mechanics, epidemiology, population ecology, and neuroscience. More advanced GNN architecture is perhaps necessary for these applications, such as stacking GNN layers or attention-based message aggregation. One straightforward next step is to study PGMs with more complicated couplings, for instance a multivariate von Mises distribution whose pairwise

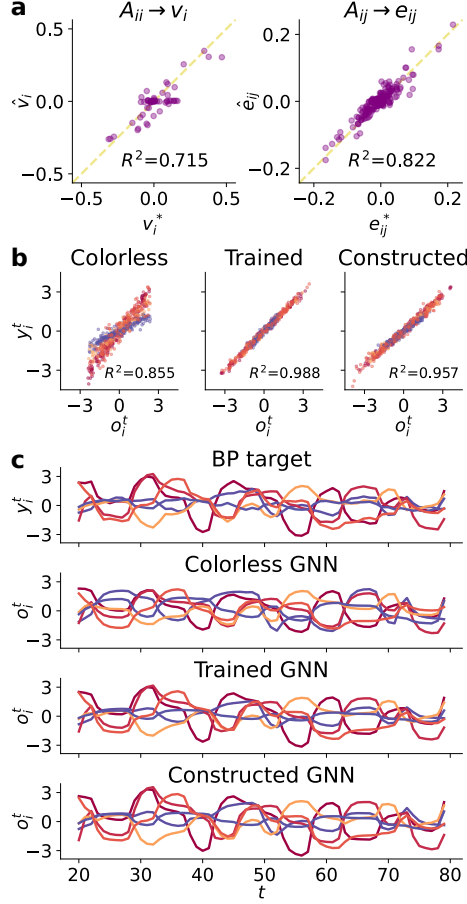


Figure 9: Translating a precision matrix to GNN graph parameters. (a) Comparison of graph parameters between the constructed GNN (\hat{v}_i , \hat{e}_{ij}) and the trained GNN (v_i^* , e_{ij}^*). (b) BP targets against GNN outputs for the colorless GNN ($D_v = D_e = 0$), the trained GNN and the translated GNN. Data is colored by vertices. (c) An example trial comparing the BP target and GNN outputs, only 6 random variables are shown for clarity.

potential $\psi_{ij}(\theta_i, \theta_j)$ is specified by 4 free parameters. We predict that GNN edge dimension D_e has to be at least 4 to faithfully model BP traces on such PGMs.

In this study, we make zero assumption about the connectivity of the underlying graph, which leaves us to choose either a null graph or a fully connected one. However the connectivity can also be learned in principle if proper inductive bias is imposed, *e.g.* a sparsity prior, proximity rules, etc. In fact, one can try to estimate the connectivity from the learned fully connected edge parameters e_{ij} and use these estimates as the graph's edges \mathcal{E} for the next iteration of GNN training. Approaches that learn connectivity end-to-end should also be explored.

From fitting quality alone, we obtain a basic picture on the dimensions of the complex system (Fig. 3), but identification of the exact values of D_v , D_e , D_s and D_m is still an open question. Preliminary data suggests that it is possible to identify them using generalization performance on new instances (Fig. 9) as a metric. Only the GNNs with correct assumptions about dimensions can accurately predict system behavior on a new instance, because either underestimation or overestimation will result ‘incorrectly’ constructed GNNs. We will examine the results further, also include $D_v = 1$ and $D_e = 1$ in the architecture search.

For simplicity, we use a canonical readout (Eq. 4) in this study, assuming the number of parts in the system is known and they are observed separately in the same manner. But in some real problems the assumption does not hold, observations of the system can be a mixed representation of all parts (Eq. 5), *e.g.* the cortical representation of a visual scene. How to use GNNs to understand dynamics and structure of the system from mixed observation is something we plan to investigate in the future.

References

- [1] F. Scarselli, M. Gori, A. C. Tsoi, M. Hagenbuchner, and G. Monfardini. The graph neural network model. *IEEE Transactions on Neural Networks*, 20(1):61–80, Jan 2009.
- [2] Yujia Li, Daniel Tarlow, Marc Brockschmidt, and Richard Zemel. Gated graph sequence neural networks. In *In Proceedings of the International Conference on Learning Representations*, 11 2016.
- [3] Peter W. Battaglia, Jessica B. Hamrick, Victor Bapst, Alvaro Sanchez-Gonzalez, Vinicius Zambaldi, Mateusz Malinowski, Andrea Tacchetti, David Raposo, Adam Santoro, Ryan Faulkner, Caglar Gulcehre, Francis Song, Andrew Ballard, Justin Gilmer, George Dahl, Ashish Vaswani, Kelsey Allen, Charles Nash, Victoria Langston, Chris Dyer, Nicolas Heess, Daan Wierstra, Pushmeet Kohli, Matt Botvinick, Oriol Vinyals, Yujia Li, and Razvan Pascanu. Relational inductive biases, deep learning, and graph networks. *ArXiv e-prints*, Jun 2018.
- [4] Zhitao Ying, Jiaxuan You, Christopher Morris, Xiang Ren, Will Hamilton, and Jure Leskovec. Hierarchical graph representation learning with differentiable pooling. In S. Bengio, H. Wallach, H. Larochelle, K. Grauman, N. Cesa-Bianchi, and R. Garnett, editors, *Advances in Neural Information Processing Systems*, volume 31. Curran Associates, Inc., 2018.
- [5] Justin Gilmer, Samuel S. Schoenholz, Patrick F. Riley, Oriol Vinyals, and George E. Dahl. Neural message passing for quantum chemistry. In Doina Precup and Yee Whye Teh, editors, *Proceedings of the 34th International Conference on Machine Learning*, volume 70 of *Proceedings of Machine Learning Research*, pages 1263–1272, International Convention Centre, Sydney, Australia, 06–11 Aug 2017. PMLR.
- [6] Nicholas Watters, Daniel Zoran, Theophane Weber, Peter Battaglia, Razvan Pascanu, and Andrea Tacchetti. Visual interaction networks: Learning a physics simulator from video. In I. Guyon, U. V. Luxburg, S. Bengio, H. Wallach, R. Fergus, S. Vishwanathan, and R. Garnett, editors, *Advances in Neural Information Processing Systems*, volume 30. Curran Associates, Inc., 2017.
- [7] Thomas Kipf, Ethan Fetaya, Kuan-Chieh Wang, Max Welling, and Richard Zemel. Neural relational inference for interacting systems. *ArXiv e-prints*, February 2018.
- [8] Peter Battaglia, Razvan Pascanu, Matthew Lai, Danilo Jimenez Rezende, and koray kavukcuoglu. Interaction networks for learning about objects, relations and physics. In D. D. Lee, M. Sugiyama, U. V. Luxburg, I. Guyon, and R. Garnett, editors, *Advances in Neural Information Processing Systems* 29, pages 4502–4510. Curran Associates, Inc., 2016.
- [9] V. Bapst, T. Keck, A. Grabska-Barwińska, C. Donner, E. D. Cubuk, S. S. Schoenholz, A. Obika, A. W. R. Nelson, T. Back, D. Hassabis, and P. Kohli. Unveiling the predictive power of static structure in glassy systems. *Nature Physics*, 16(4):448–454, 2020.
- [10] Miles Cranmer, Alvaro Sanchez-Gonzalez, Peter Battaglia, Rui Xu, Kyle Cranmer, David Spergel, and Shirley Ho. Discovering symbolic models from deep learning with inductive biases. *arXiv e-prints*, June 2020.
- [11] Petar Veličković, Guillem Cucurull, Arantxa Casanova, Adriana Romero, Pietro Liò, and Yoshua Bengio. Graph attention networks. In *International Conference on Learning Representations*, 2018.
- [12] Renjie Liao, Yujia Li, Yang Song, Shenlong Wang, Will Hamilton, David K Duvenaud, Raquel Urtasun, and Richard Zemel. Efficient graph generation with graph recurrent attention networks. *Advances in Neural Information Processing Systems*, 32:4255–4265, 2019.
- [13] Kevin P. Murphy, Yair Weiss, and Michael I. Jordan. Loopy belief propagation for approximate inference: An empirical study. In *Proceedings of the Fifteenth Conference on Uncertainty in Artificial Intelligence*, UAI’99, page 467–475, San Francisco, CA, USA, 1999. Morgan Kaufmann Publishers Inc.
- [14] M.J. Wainwright, T.S. Jaakkola, and A.S. Willsky. Tree-based reparameterization framework for analysis of sum-product and related algorithms. *IEEE Transactions on Information Theory*, 49(5):1120–1146, 2003.
- [15] Michael Chang, Tomer Ullman, Antonio Torralba, and Joshua B. Tenenbaum. A compositional object-based approach to learning physical dynamics. In *5th International Conference on Learning Representations, ICLR 2017, Toulon, France, April 24-26, 2017, Conference Track Proceedings*. OpenReview.net, 2017.
- [16] Alvaro Sanchez-Gonzalez, Jonathan Godwin, Tobias Pfaff, Rex Ying, Jure Leskovec, and Peter Battaglia. Learning to simulate complex physics with graph networks. In Hal Daumé III and Aarti Singh, editors, *Proceedings of the 37th International Conference on Machine Learning*, volume 119 of *Proceedings of Machine Learning Research*, pages 8459–8468. PMLR, 13–18 Jul 2020.
- [17] Meng Qu, Yoshua Bengio, and Jian Tang. GMNN: Graph Markov neural networks. In Kamalika Chaudhuri and Ruslan Salakhutdinov, editors, *Proceedings of the 36th International Conference on Machine Learning*, volume 97 of *Proceedings of Machine Learning Research*, pages 5241–5250. PMLR, 09–15 Jun 2019.

- [18] Victor Garcia Satorras, Zeynep Akata, and Max Welling. Combining generative and discriminative models for hybrid inference. *Advances in Neural Information Processing Systems*, 32:13825–13835, 2019.
- [19] KiJung Yoon, Renjie Liao, Yuwen Xiong, Lisa Zhang, Ethan Fetaya, Raquel Urtasun, Richard Zemel, and Xaq Pitkow. Inference in probabilistic graphical models by graph neural networks. In *2019 53rd Asilomar Conference on Signals, Systems, and Computers*, pages 868–875. IEEE, 2019.
- [20] Zhen Zhang, Fan Wu, and Wee Sun Lee. Factor graph neural network. *arXiv preprint arXiv:1906.00554*, 2019.
- [21] Yicheng Fei and Xaq Pitkow. Generalization of graph network inferences in higher-order probabilistic graphical models. *arXiv preprint arXiv:2107.05729*, 2021.
- [22] Kyunghyun Cho, Bart van Merriënboer, Caglar Gulcehre, Dzmitry Bahdanau, Fethi Bougares, Holger Schwenk, and Yoshua Bengio. Learning phrase representations using RNN encoder–decoder for statistical machine translation. In *Proceedings of the 2014 Conference on Empirical Methods in Natural Language Processing (EMNLP)*, pages 1724–1734. Association for Computational Linguistics, 2014.
- [23] Danny Bickson. *Gaussian belief propagation: theory and application*. PhD thesis, The Hebrew University of Jerusalem, Nov 2009.
- [24] Yair Weiss and William T Freeman. Correctness of belief propagation in gaussian graphical models of arbitrary topology. *Neural computation*, 13(10):2173–2200, 2001.

A Meta-MLP

We design a family of MLPs organized by meta-parameters, called meta-MLP or mMLP for short. In an original MLP, the input vector \mathbf{x} is defined as layer 0 activation \mathbf{x}^0 . L sequential perceptrons transform activation from one layer to the next by

$$\mathbf{x}^l = f^l \left(\mathbf{W}^l \mathbf{x}^{l-1} + \mathbf{b}^l \right), \quad (13)$$

in which \mathbf{W}^l and \mathbf{b}^l are the weight and bias of layer l respectively, and $f^l(\cdot)$ is the nonlinear activation function of layer l . The L -th layer activation \mathbf{x}^L is defined as the output of the MLP,

$$\text{MLP}(\mathbf{x}; \Theta) \equiv \mathbf{x}^L, \quad (14)$$

with $\Theta = \{\mathbf{W}^1, \mathbf{b}^1, \dots, \mathbf{W}^L, \mathbf{b}^L\}$.

In an mMLP with meta-parameter ζ , each layer is defined as

$$\mathbf{x}^{l+1} = f^l \left(\mathbf{W}^l \begin{bmatrix} \mathbf{x}^l \\ \zeta \end{bmatrix} + \mathbf{b}^l \right). \quad (15)$$

In Eq. 15, the meta-parameter ζ modulates each layer transformation by acting as an extra input. The output of the mMLP is defined as the last layer activation

$$\text{mMLP}(\mathbf{x}, \zeta; \Theta) \equiv \mathbf{x}^L. \quad (16)$$

Optionally, batch normalization layers can be added right before each nonlinear activation function. When a batch normalization layer with trainable affine transformation is added, the bias \mathbf{b}^l will be removed.

In this study, all layers in an mMLP except the last one use the nonlinear ELU activation, *i.e.*

$$f^l(z) = \begin{cases} z & z \geq 0, \\ e^z - 1 & z < 0, \end{cases} \quad (17)$$

for $1 \leq l < L$. The activation function of last layer is the identity function $f^L(z) = z$.

B Canonical functions

B.1 Message function

In this study, the message function $\mathcal{M}(\cdot)$ is defined as

$$\mathcal{M}(\mathbf{s}_i^t, \mathbf{s}_j^t; \mathbf{e}_{ij}, \Theta_{\mathcal{M}}) \equiv \text{mMLP} \left(\begin{bmatrix} \mathbf{s}_i^t \\ \mathbf{s}_j^t \end{bmatrix}, \mathbf{e}_{ij}; \Theta_{\mathcal{M}} \right). \quad (18)$$

While message parameter $\Theta_{\mathcal{M}}$ is shared across all edges, meta-parameter \mathbf{e}_{ij} are different for different edges.

B.2 Update function

We use a modified version of gated recurrent unit (GRU) function [22] as the update function $\mathcal{U}(\cdot)$ (Eq. 1). The form of original GRU update is

$$\begin{aligned}\mathbf{z}^t &= \sigma_g (\mathbf{W}_z \mathbf{x}^t + \mathbf{U}_z \mathbf{s}^t + \mathbf{b}_z), \\ \mathbf{r}^t &= \sigma_g (\mathbf{W}_r \mathbf{x}^t + \mathbf{U}_r \mathbf{s}^t + \mathbf{b}_r), \\ \mathbf{s}^{t+1} &= (1 - \mathbf{z}^t) \circ \mathbf{s}^t + \mathbf{z}^t \circ \sigma_s (\mathbf{W}_s \mathbf{x}^t + \mathbf{U}_s (\mathbf{r}^t \circ \mathbf{s}^t) + \mathbf{b}_h),\end{aligned}$$

in which \mathbf{x}^t and \mathbf{s}^t are the external input and hidden state at time t respectively. \mathbf{z}^t and \mathbf{r}^t are the update gate and reset gate vectors, while $\sigma_g(\cdot)$ and $\sigma_s(\cdot)$ are nonlinear functions typically chosen as logistic function and hyperbolic tangent function respectively.

While original GRU uses perceptrons for gates and state updates, we replace them by meta-MLPs with vertex parameter \mathbf{v}_i . We do not append nonlinear activation to the last layer of mMLP (Appendix A), hence the gating nonlinearities σ_g and σ_s are kept. Another difference is each vertex receives not only external input, but also aggregated messages from neighbors. The update function $\mathcal{U}(\cdot)$ (Eq. 3) is defined through

$$\mathbf{z}_i^t = \sigma_g \left(\text{mMLP} \left(\begin{bmatrix} \mathbf{i}_i^t \\ \mathbf{m}_i^t \\ \mathbf{s}_i^t \end{bmatrix}, \mathbf{v}_i; \Theta_{\mathcal{U}^z} \right) \right), \quad (19)$$

$$\mathbf{r}_i^t = \sigma_g \left(\text{mMLP} \left(\begin{bmatrix} \mathbf{i}_i^t \\ \mathbf{m}_i^t \\ \mathbf{s}_i^t \end{bmatrix}, \mathbf{v}_i; \Theta_{\mathcal{U}^r} \right) \right), \quad (20)$$

$$\mathbf{s}_i^{t+1} = (1 - \mathbf{z}_i^t) \circ \mathbf{s}_i^t + \mathbf{z}_i^t \circ \sigma_s \left(\text{mMLP} \left(\begin{bmatrix} \mathbf{i}_i^t \\ \mathbf{m}_i^t \\ \mathbf{s}_i^t \end{bmatrix}, \mathbf{v}_i; \Theta_{\mathcal{U}^s} \right) \right). \quad (21)$$

The update parameter is defined as $\Theta_{\mathcal{U}} = \Theta_{\mathcal{U}^z} \cup \Theta_{\mathcal{U}^r} \cup \Theta_{\mathcal{U}^s}$.

B.3 Readout function

We choose a simple linear function as canonical readout $\mathcal{R}(\cdot)$ (Eq. 4),

$$\mathcal{R}(\mathbf{s}_i^t; \Theta_{\mathcal{R}}) = \mathbf{W}_{\mathcal{R}} \mathbf{s}_i^t + \mathbf{b}_{\mathcal{R}}, \quad (22)$$

with readout parameter $\Theta_{\mathcal{R}} = \{\mathbf{W}_{\mathcal{R}}, \mathbf{b}_{\mathcal{R}}\}$.

C Noisy belief propagation algorithm

We use belief propagation (BP) algorithm to estimate the marginal distribution of all variables. We define the message from vertex j to i as $m_{ij}(\theta_i)$, namely the belief about i from j . At each iteration, BP updates $m_{ij}(\theta_i)$ to

$$m_{ij}(\theta_i) = \frac{\tilde{m}_{ij}(\theta_i)}{\sum_{\theta_i} \tilde{m}_{ij}(\theta_i)}, \quad (23)$$

$$\tilde{m}_{ij}(\theta_i) = \sum_{\theta_j} \left(\phi_j(\theta_j) \psi_{ij}(\theta_i, \theta_j) \prod_{k \in N(j) \setminus i} m_{jk}(\theta_j) \right), \quad (24)$$

in which $N(j)$ is the set of neighbors of j . The marginal distribution of θ_i is

$$p_i(\theta_i) = \frac{\tilde{p}_i(\theta_i)}{\sum_{\theta_i} \tilde{p}_i(\theta_i)}, \quad (25)$$

$$\tilde{p}_i(\theta_i) = \phi_i(\theta_i) \prod_{j \in N(i)} m_{ij}(\theta_i). \quad (26)$$

We explicitly normalize messages and estimated marginal distributions at each iteration.

BP is not guaranteed to converge on loopy graphs, even when it converges it may not converge to the true marginal distribution. However if damping update is used, BP usually gives a stable good approximation and can be considered

as a valid inference algorithm. We denote the damping coefficient as γ . BP updates messages in logarithm domain following

$$m_{ij}^t(\theta_i) = \frac{\tilde{m}_{ij}^t(\theta_i)}{\sum_{\theta_i} \tilde{m}_{ij}^t(\theta_i)}, \quad (27)$$

$$\ln(\tilde{m}_{ij}^{t+1}(\theta_i)) = \gamma \ln(m_{ij}^t(\theta_i)) + (1 - \gamma) \ln \left(\sum_{\theta_j} \left(\phi_j^t(\theta_j) \psi_{ij}(\theta_i, \theta_j) \prod_{k \in N(j) \setminus i} m_{jk}^t(\theta_j) \right) \right), \quad (28)$$

with superscript t marks the time step in BP. Here the singleton potential $\phi_i^t(\theta_i)$ changes over time. Similarly, the estimated marginal distribution is also dynamic,

$$p_i^t(\theta_i) = \frac{\tilde{p}_i^t(\theta_i)}{\sum_{\theta_i} \tilde{p}_i^t(\theta_i)}, \quad (29)$$

$$\tilde{p}_i^t(\theta_i) = \frac{1}{Z} \phi_i^t(\theta_i) \prod_{j \in N(i)} m_{ij}^t(\theta_i). \quad (30)$$

We additionally add processing noise to the inference algorithm to mimic a physical system. Since the message by definition is non-negative, we use additive noise in logarithmic domain to distort each update step. The complete form is

$$\ln(m_{ij}^t(\theta_i)) + (1 - \gamma) \ln \left(\sum_{\theta_j} \left(\phi_j^t(\theta_j) \psi_{ij}(\theta_i, \theta_j) \prod_{k \in N(j) \setminus i} m_{jk}^t(\theta_j) \right) \right) + n_i^t, \quad (31)$$

in which $n_i^t \sim \mathcal{N}(0, \sigma_n^2)$ is independent Gaussian noise with variance σ_n^2 .

D Trace data

BP traces are generated for 36 PGMs. For each PGM, its graph size is randomly sampled from $\{12, 14, 16, 18\}$, the BP duration is randomly sampled from $\{80, 100, 120\}$, and the number of trials is randomly sampled from $\{1000, 1250, 1500\}$. Precision matrix of each PGM is a random positive-definite matrix, generated by applying random rotations on a subset of indices starting from a diagonal matrix until desired density is reached (similar to ‘sprandsym’ function in MATLAB). The reciprocal condition number is 0.2, and the desired density is 60% (estimated using a threshold of $\epsilon = 0.01$ when the starting diagonal matrix has maximum value of 1).

The full dataset includes approximately 75 million data points (graph size \times duration \times number of trials, summed up for all 36 PGMs). 90%, 5% and 5% of the data are used for training, validation and testing respectively.

E Example trial of the best GNN

An example trial of the best fit GNN (Fig. 3b) is shown in Fig. 10.

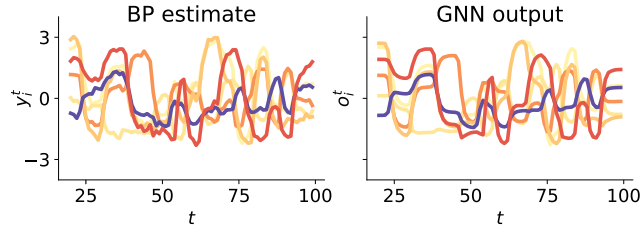


Figure 10: An example trial of the first six random variables of one PGM. The input sequence is from a held-out testing set.

Since no processing noise is introduced in GNN, its output is smoother than the target traces given by noisy BP algorithm. The trained GNN captures main component of observed dynamical data, effectively removing the noise within.

F PCA on aggregated messages

PCA is performed on the aggregated messages \mathbf{m}_i^t (Eq. 2) for the trained GNN. Similar to the geometry of states \mathbf{s}_i^t (Fig. 4), aggregated messages for each vertex also lie on a curved 1-D manifold in the high-dimensional space.

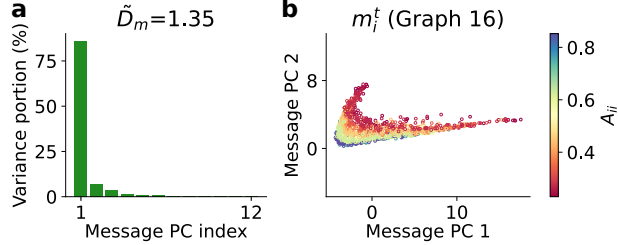


Figure 11: Manifold analysis of aggregated messages. (a) PCA spectrum of aggregated messages \mathbf{m}_i^t in the example GNN. (b) 2D visualization of \mathbf{m}_i^t , colored by the precision matrix of each vertex.

G Training with no regularization

When no regularization is added on structural parameters \mathbf{v}_i and \mathbf{e}_{ij} , the trained GNN can still predict BP traces well. One of the best architectures we found is $D_e = 8$, $D_v = 4$, $D_h = 12$, $D_h = 12$ and a message function with two hidden layers of size [32, 16]. Though the its fitting performance is high ($R^2 = 0.989$), PCA on the learned \mathbf{v}_i and \mathbf{e}_{ij} does not reveal low-dimensional manifold.

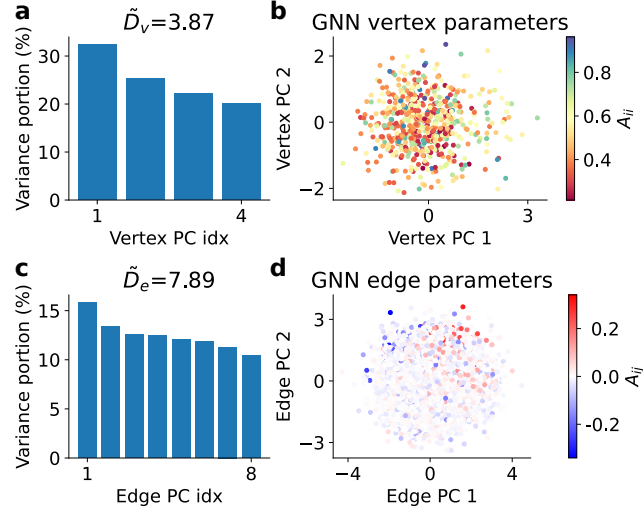


Figure 12: Learned structural parameters with no regularization. (a) PCA spectrum of \mathbf{v}_i when $D_v = 4$. (b) 2D visualization of \mathbf{v}_i colored by A_{ii} . (c) PCA spectrum of \mathbf{e}_{ij} when $D_e = 12$. (d) 2D visualization of \mathbf{e}_{ij} colored by A_{ij} .

However, PCA on the states and pairwise messages of the trained GNNs still show low-dimensional structure, similar to Fig. 4 and Fig. 5. In fact, the messages seem to be more organized as the 1-D manifolds belonging to different edges are aligned parallel.

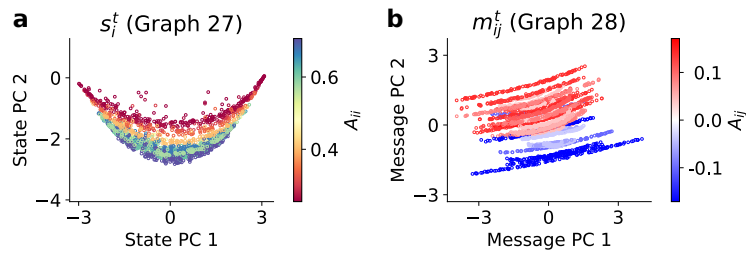


Figure 13: PCA of GNN states and messages when no regularization is used during training. (a) Projection of states s_i^t onto the space spanned by its first two PCs, colored by precision parameter A_{ii} (b) Projection of messages m_{ij}^t onto the space spanned by its first two PCs, colored by coupling strength A_{ij} .